Analyst

Accepted Manuscript

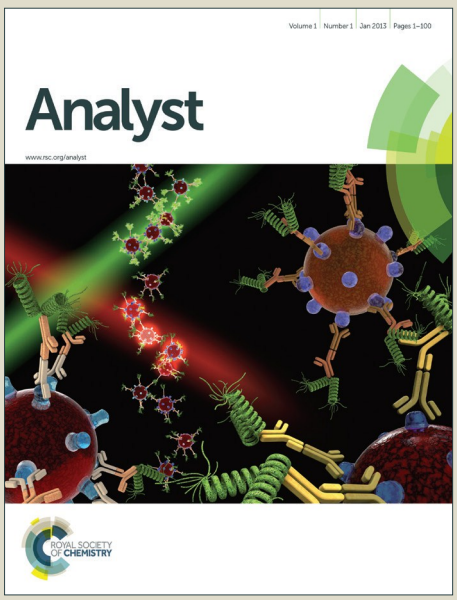

ROYAL SOCIETY OF CHEMISTRY

www.rsc.org/analyst

Journal Name

ARTICLE

Sensing protein antigen and microvesicle analytes using high-capacity biopolymer nano-carriers

Received 00th January 20xx,
Accepted 00th January 20xx

DOI: 10.1039/x0xx00000x

www.rsc.org/

Saroj Kumar,‡[ac] Gloria Milani,‡[b] Hideyo Takatsuki,‡[a] Tobia Lana,[b] Malin Persson,[a] Chiara Frasson,[b] Geertruy te Kronnie,[b] and Alf Mansson*[a]

Lab-on-a-chip systems with molecular motor driven transport of analytes attached to cytoskeletal filament shuttles (actin filaments, microtubules) circumvent challenges with nanoscale liquid transport. However, the filaments have limited cargo-carrying capacity and limitations either in transportation speed (microtubules) or control over motility direction (actin). To overcome these constraints we here report incorporation of covalently attached antibodies into self-propelled actin bundles (nanocarriers) formed by cross-linking antibody conjugated actin filaments via fascin, a natural actin-bundling protein. We demonstrate high maximum antigen binding activity and propulsion by surface adsorbed myosin motors. Analyte transport capacity is tested using both protein antigens and microvesicles, a novel class of diagnostic markers. Increased incubation concentration with protein antigen in the 0.1-100 nM range (1 min) reduces the fraction of motile bundles and their velocity but maximum transportation capacity of > 1 antigen per nm of bundle length is feasible. At sub-nanomolar protein analyte concentration, motility is very well preserved opening for orders of magnitude improved limit of detection using motor driven concentration on nanoscale sensors. Microvesicle-complexing to monoclonal antibodies on the nanocarriers compromises motility but nanocarrier aggregation via microvesicles show unique potential in label-free detection with the aggregates themselves as non-toxic reporter elements.

Introduction

Cheap, rapid and sensitive methods for diagnostics of disease using simple blood or urine samples aid strategies to overcome accelerating health care costs. In this context, there is growing interest to develop lab-on-a-chip devices[1-3] where a series of analyses are performed on a single chip. These devices are preferably integrated with nanoscale sensors for optimal sensitivity and multiplexing capabilities[4] e.g. to detect a panel of analytes/biomarkers (proteins, nucleic acid fragments, exosomes, microvesicles etc.). However, despite significant progress,[2] existing devices often use expensive and bulky accessory equipment[2, 3] including pumps for driving liquid flow. Moreover, liquid flow does not overcome limitations associated with diffusion of biomarkers to nanoscale detectors.[4] Other potential problems include biosafety issues[5] e.g. related to the use of potentially toxic inorganic nanostructures as reporter elements signaling the presence of analyte molecules.

In order to circumvent the above problems, lab-on-a-chip systems with molecular motor driven transport have been proposed.[6-11] In some tested versions of such arrangements, recognition molecules, e.g. antibodies[12-14] or oligonucleotides[15, 16] are attached to cytoskeletal filaments (actin filaments and microtubules) that are propelled by molecular motors for nanoseparation and concentration on a detector area.[8, 17, 18] Importantly, due to self-propelling features of the system (driven by turnover of adenosine-5'-triphosphate, ATP), these motor-propelled cytoskeletal shuttles[19] do not require external pumps. Furthermore, they capture biomarkers from a large solution volume and actively transport them to the detector,[6, 8, 9] thereby overcoming diffusion limitations. In addition, the detection may be achieved in unique ways, e.g. by observations of co-localization and co-transportation of filaments and biomarkers[12, 20-22] or by aggregation of the cytoskeletal filaments via analyte.[10, 23] Due to the large number of fluorescent dye molecules that may be attached to each filament, aggregates are readily detected without labeling with e.g. fluorescent, and potentially toxic, nanoparticles.

Both the actin and myosin II motor system (underlying muscle contraction) and the kinesin or dynein and microtubule systems (underlying intracellular transport) have been

[a] Department of Chemistry and Biomedical Sciences, Linnaeus University, SE-391 82 Kalmar, Sweden. E-mail: alf.mansson@lnu.se
[b] Department of Women's and Children's Health, University of Padova, 35128 Padova, Italy.
[c] Present address: Department of Biotechnology, Delhi Technological University, Delhi-110042, India.

†Electronic Supplementary Information (ESI) available: Materials and methodological details including protein preparations, preparation of flow cells, antibody conjugation to actin, in vitro motility assays and formation and characterization of antibody-labeled fascin-actin bundles, CD45 expression: screening of cell lines and MVs isolation, MVs isolation and preservation in MOPS buffer, optimization of CFSE staining and extended MV shelf-life. Furthermore, supplementary figures and movies are included. See DOI: 10.1039/x0xx00000x

‡ Authors contributed equally to this work.

explored in work towards motor driven lab-on-a-chip devices (cf.[12, 20-22]; reviewed in[10, 24]) each with different advantages and challenges.[10] The actin filaments thus exhibit ten-fold higher speed with rapid transport to a detector site[10, 18] whereas microtubule based transport may be more robust against cargo induced disturbances.[10] Furthermore, the higher flexural rigidity of microtubules facilitates guiding along microfabricated tracks[25] and enhances concentration on a detector.[18, 26]

For both the microtubule- and actin-based system, antibodies have been covalently attached to single filaments but it would be desirable to increase the total number of active antibodies on the surface of each nanocarrier.[14] For optimized molecular motor driven lab-on-a-chip devices it is also of interest to combine the advantages of the microtubule and actin based systems. It has been suggested[27-29] that this should be possible using unipolar bundles of actin filaments formed by cross-linking via fascin, the protein that underlies actin-bundling in filopodia at the leading end of motile cells. The fascin-actin bundles exhibit high flexural rigidity similar to that of microtubules[28, 30, 31] but are propelled by myosin motors at similar high velocity as individual actin filaments. The bundles also have the capacity to carry cell-sized cargoes without disturbances in motility.[27] However, only streptavidin-biotin links have been tested for cargo attachment with biotin non-covalently attached to the actin filament via phalloidin.[27, 29] This approach cannot form the basis for a practically useful device because the phalloidin-actin binding is reversible with a dissociation half-time of around 20 min.[32] It is, on the other hand, not clear whether covalent antibody-conjugated actin filaments[14] can be incorporated into bundles together with fascin. Furthermore, if this turns out to be possible it is not self-evident that such a construct maintains self-propulsion and antigen binding.

Here we first demonstrate successful incorporation of covalently antibody-conjugated actin filaments into fascin-actin bundles with well-preserved self-propulsion and an unprecedented maximum capacity to bind and transport protein antigens. The use of this novel nanocarrier allowed 10-fold improvement in the signal-to-noise ratio for fluorescence detection of protein antigens compared to single actin filaments. We also studied binding and transport of microvesicles (MVs), an emerging class of biomarkers in the form of lipid vesicles (100-1000 nm) that are pinched off from living cells in physiological and pathological conditions.[33] The MVs exhibit appreciable potential as biomarkers in cancer and other diseases.[34-38 39-42] Here, we found that MVs released by cells positive for CD45 antigen were captured by actin filaments and actin filament bundles functionalized with anti-CD45 monoclonal antibodies. Even if nanocarrier based transportation of the MVs was challenging, the capacity to capture the MVs opens for novel label-free sensing schemes based on aggregation of fluorescent actin filaments or fascin-actin bundles.[23]

Results and Discussion

We report findings at the interface of biology, chemistry, materials science and clinical medicine. A key element is production of a novel self-propelled nanomaterial, a nanocarrier, where covalent conjugation of antibodies to actin filaments is combined with self-assembly of the filaments by specific biomolecular recognition using actin-binding proteins as cross-linkers. We evaluate the performance of the nanocarrier in capturing, transporting and detecting protein antigens as well as microvesicles, a novel class of clinically relevant biomarkers.

Assembly of nanocarrier and capture of protein antigen

Actin filaments were first covalently conjugated with antibodies, either polyclonal anti-rabbit IgG (a-rIgG) or monoclonal anti-CD45 (a-CD45), using hetero-bifunctional cross-linkers.[14, 43-45] These antibody conjugated filaments formed bundles upon mixing with the actin-binding protein fascin[28, 31] (Fig. 1). The success of this approach was somewhat surprising in view of appreciably larger molecular weight (~150 kDa) of the antibodies than of fascin (~57 kDa) and also a shape (Y-shape) with expected larger effective space occupancy. However, the actin-fascin bundles with antibodies contained only 7.3 ± 2.2 filaments (mean ± 95% CI; N=10 bundles), lowered ($p<0.05$; t-test) to 4.1 ± 1.7 filaments (N=10) approximately 5 min after ATP addition due to bundle disassembly (size distributions in Fig. S1†). Simultaneously, the bundle fraction was reduced from 15.3 and 14.6 % to 7.6 and 10.6 %, respectively, in two experiments, reducing the fraction of filaments incorporated into bundles from close to 60 % to about 30 %. The bundle size was less than without antibodies (~20)[28, 31, 46]. However, antigen-binding to antibodies seemed to reduce the ATP-induced disassembly, possibly due to cross-linking of neighbouring filaments via antigen. For instance, the average observed bundle size 5 min after ATP-addition was 6.4 ± 2.2 (N=30) in the presence of 1 nM rhodamine labeled rabbit IgG (Rh-rIgG).

Successful incorporation of a-rIgG conjugated actin filaments (also Alexa Fluor®-488 phalloidin (APh) labeled) into fascin-actin bundles was verified using fluorescence microscopy (Fig. 2a-d; Fig. S2†) after immobilizing bundles to a surface coated with heavy meromyosin (HMM) in the absence of ATP. For this purpose we used fluorescent rabbit IgG (Rh-rIgG) as antigen. Binding of Rh-rIgG to a-rIgG-actin was observed both for individual actin filaments and fascin-actin-bundles following 1 min of incubation (Fig. 2). The results imply effective incorporation of antibody-functionalized actin filaments into the bundles as well as effective antigen binding of these antibodies.

Evaluation on basis of Rh-rIgG fluorescence intensity (Fig. 2e,f) showed a concentration-dependent increase in the fraction of bundles (independent of size) and single filaments with observed Rh-rIgG labeling. The concentration dependence of the binding was also reflected in increased stoichiometric ratio of Rh-rIgG to actin.

Journal Name

ARTICLE

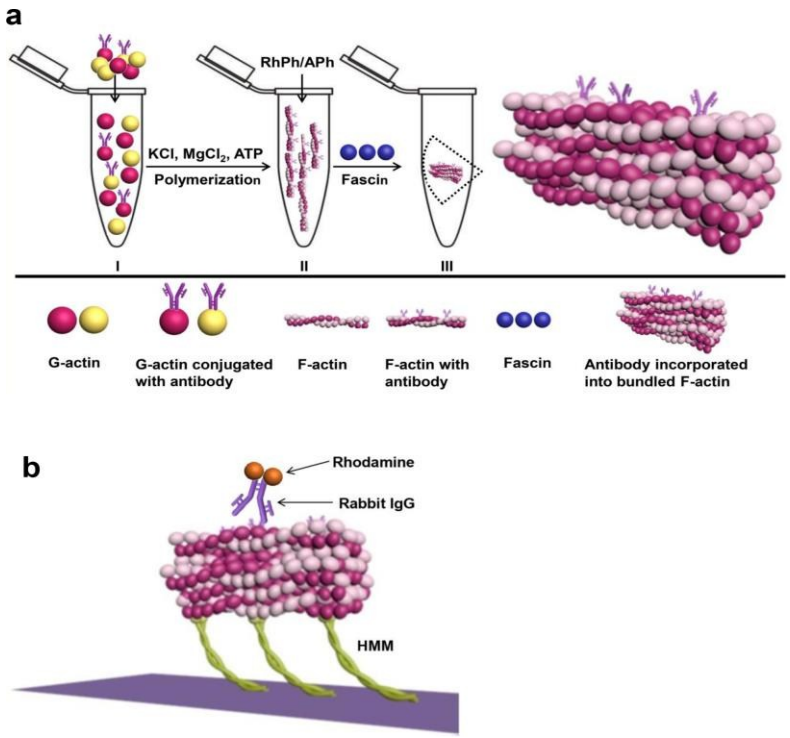

Fig. 1 Schematic illustration of the formation of fascin-actin bundles with antibodies and subsequent transportation of antige (Rh-rIgG) captured by antibodies. (a) Bundle formation from antibody-conjugated G-actin monomers (I) via actin filaments (II) and finally, assembled bundles (III). (b) HMM driven transport of Rh-rIgG antigen captured by anti-rabbit IgG antibody

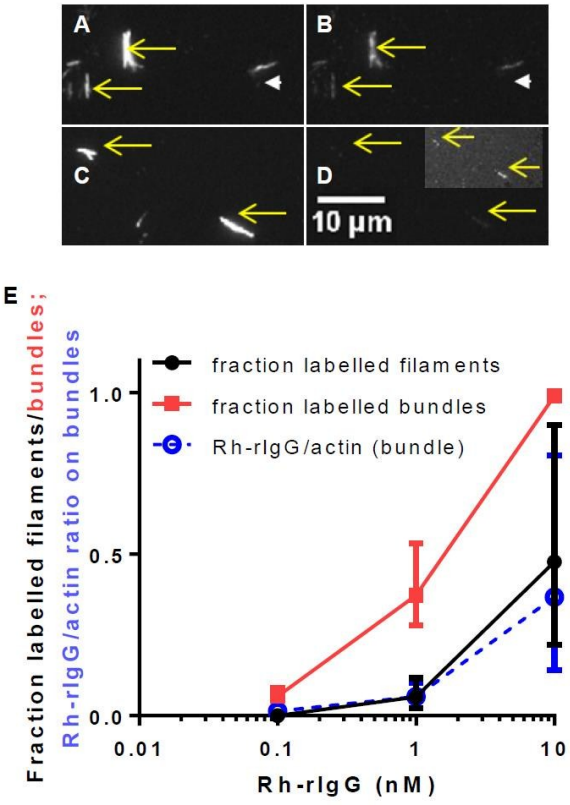

Fig. 2 Capture of Rh-rIgG antigen by APh labeled actin filaments and fascin-actin bundles. **(**a, c) APh labeling observed using a fluorescein isothiocyanate (FITC) filter set in epi-fluorescence microscope. (b) Same region as in (a) a few seconds later after switch to a tetramethyl rhodamine isothiocyanate (TRITC) filter set for observation of Rh-rIgG antigens (incubation with 10 nM for 1 min) captured by a-rIgG antibodies on filaments and bundles. (d) Same region as in (c) a few seconds later after switch to TRITC filter set for observation of Rh-rIgG antigens (incubation with 1 nM for 1 min) on bundles. *Inset.* After histogram stretching for maximum contrast and brightness. Full length arrows indicate bundles whereas arrow-heads indicate occasional single actin filaments. Similar exposure time and gain in (a) and (b) (exposure time 0.1 s) and in (c) and (d) (0.4 s). The filaments and bundles are bound to a trimethylchlorosilane (TMCS) derivatized surface coated with HMM in the absence of ATP. (e) The fraction of isolated actin filaments (circles, black) and fascin-actin bundles (squares, red) with Rh-rIgG labeling and the Rh-rIgG/actin stochiometric ratio for the 2-4 bundles with most extensive Rh-rIgG labeling (blue open circles). Incubation time, 1 min. Data from 3 independent experiments at each Rh-rIgG concentration. Error bars: range.

Journal Name

ARTICLE

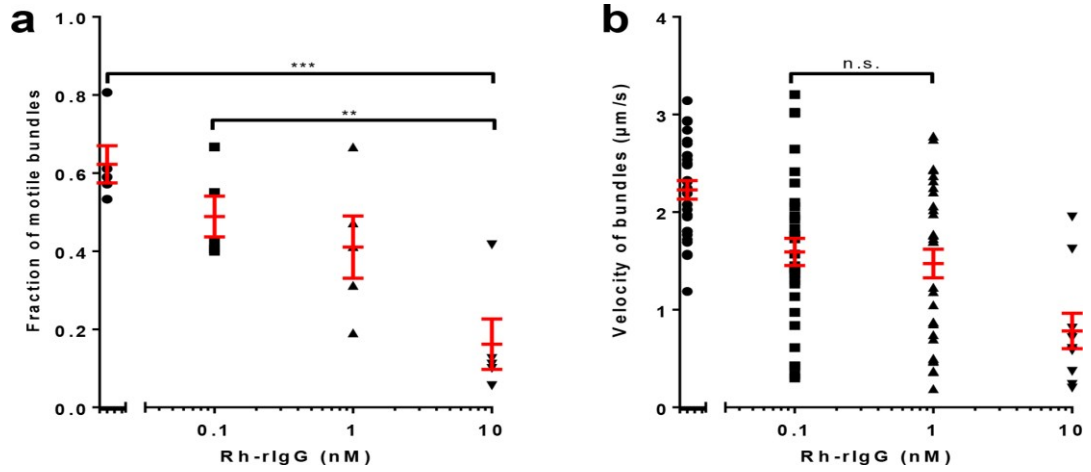

Fig. 3 Effect of increasing Rh-rIgG incubation concentration on motility quality of fascin-crosslinked bundles composed of anti-rabbit-IgG-conjugated actin filaments also labeled with APh. (a) The fraction of motile bundles. Individual data points (black) from five observed image frames at 3 different experimental occasions given with overall mean ± SEM (red). Significant difference between overall mean values was observed at 0 and 0.1 nM on the one hand and 10 nM on the other. ***, p<0.001, **, p<0.01. (b) Sliding velocity. Individual data points (*N*=10-31 bundles: black) at each Rh-rIgG concentration from 3 different experimental occasions given with overall mean ± SEM (red). Statistically significant difference (p<0.05) between mean values in all separate groups except in the case indicated by "n.s." Temperature, 21-23 °C. Statistical hypothesis testing was performed using one way analysis of variance (ANOVA) followed by Tukey´s post hoc test for differences between separate groups.

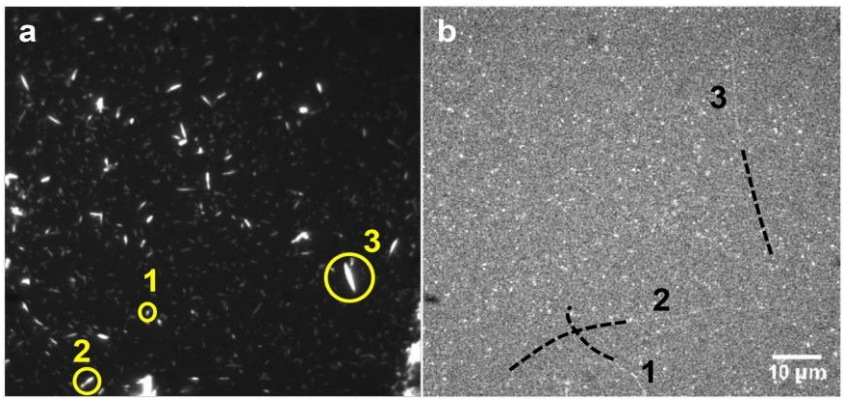

Fig. 4 Observation of motile fascin-actin bundles with captured Rh-rIgG antigen after 1 min incubation with 0.1 nM Rh-rIgG. (a) Snapshot (0.4 s) illustrating APh labeled actin filaments and fascin-actin bundles imaged using epi-fluorescence microscope and FITC filter set. Numbers and circles depict three bundles that are motile and that transport Rh-rIgG molecules as shown in (b). (b) ImageJ-derived Z-stack of same area as in (a) after shifting to TRITC filter set. This image shows the standard-deviation of the pixel intensities of 35 (0.4 s) image frames starting approximately 10 s after the snapshot in (a). The weak bright traces (1-3) indicate the motion of Rh-rIgG molecules during the 35 frame period. The dashed lines indicate the approximate paths of the Rh-rIgG-carrying bundles from the observations in (a).

Journal Name

ARTICLE

The fraction of labeled fascin-actin bundles increased from 1-5% at 0.1 nM to 100% at 10 nM Rh-rIgG, following 1 min incubation (Fig. 2e). The results demonstrate appreciably improved detection of antigen binding to bundles compared to isolated filaments with limit of detection lowered from the range 1-10 nM to 0.1-1 nM. Here, the number of Rh labeled bundles and filaments were used as relevant signals. With about 30 % or more of all filaments incorporated into bundles (see above) only limited additional improvement would be achieved by preventing bundle disassembly by further cross-linking (e.g. covalent or streptavidin-biotin based).

The degree of Rh-rIgG labeling was estimated for the most heavily Rh-rIgG labeled bundles by comparing the Rh and the APh intensity of the same bundles (see experimental section). This analysis suggests a highly variable maximum Rh-rIgG/actin stoichiometric ratio of 0.14, 0.16 and 0.80 (at 10 nM Rh-rIgG), in three independent experiments.

HMM driven transportation of captured protein antigen

We next asked whether the velocity and fraction of motile HMM propelled filaments/bundles were affected either by antibody-labeling (anti-rabbit IgG) and/or by the subsequent binding of protein antigen (Rh-rIgG). Our results (Fig. 3; Movies S1-S4†) show that the mean fraction of motile bundles and the mean sliding velocities decreased with increased Rh-rIgG concentration. Whereas most (>80%) fascin-actin bundles that were labeled with Rh-rIgG at 10 nM incubation concentration were non-motile, one bundle with > 1200 Rh-rIgG bound per µm of its length (at 0.14 actin-Rh-rIgG ratio and with ~20 actin filaments) was propelled for more than 10 µm at a velocity of 2.4 µm/s. This was more than 50% of the velocity observed for bundles in the absence of antigen and clearly demonstrates that high degree of Rh-rIgG loading does not necessarily inhibit motility.

For large bundles the motility inhibition at high Rh-rIgG binding was partly due to the formation of cross-links between differently oriented parts of the bundles via antigens (cf. Fig. S3†). On the other hand, the motility of an appreciable fraction of single filaments, particularly small fragments was also inhibited. This is related to the observation that the amount of non-specifically adsorbed antigen outside filaments and bundles was clearly increased when the Rh-rIgG concentration increased within the range 1 to 100 nM (shown for 0, 1 and 10 nM Rh-rIgG in Fig. S4†).

The effect of Rh-rIgG binding on the fraction of motile bundles was small for incubation concentrations of 0.1-1 nM and motility was observed for several bundles carrying Rh-rIgG antigen after incubation at 0.1 nM (Fig. 4). The good motility under these conditions is in accordance with very low density of Rh-rIgG, both non-specifically adsorbed to the surface and specifically bound to antibodies on the bundles. However, small but statistically significant changes in mean velocity and increased variability in velocity (Fig. 3b) suggest disturbance of motility also at low Rh-rIgG concentrations (< 1 nM). Nevertheless, we have demonstrated that actin-fascin antibody bundles show appreciable potential to function as a novel nanocarrier under several conditions.

Specific capture of CD45 positive microvesicles on actin filaments

Leukemic cell lines were screened in order to select a cell system positive for the CD45 cell surface antigen and for robust *in vitro* production of MVs with CD45 positivity similar to that of the cells. On this basis we selected the human T-cell leukemia cell line DND41 cells as positive control (CD45+) and an MG63 human osteosarcoma cell line as negative control (CD45-) (Fig. S5-S6†). MVs were isolated from both cell and checked for CD45 presence by flow cytometry (Fig. S7-S8†).

Because MV-capture has not previously been attempted using antibodies on single filaments, we first performed experiments using isolated actin filaments labeled with CD45 specific monoclonal antibodies. Experiments were performed using dilutions in the flow cell of 1/10-1/50 of standard MV preparations from cell lines giving less than 200 MVs per image frame after 5 min incubation. This includes non-specifically surface adsorbed MVs and MVs specifically captured by antibodies. The specific capturing by anti-CD45-conjugated actin filaments of CD45+ MVs, labeled with carboxyfluorescein diacetate succinimidyl ester (CFSE), was confirmed by fluorescence co-localization experiments. In these experiments (Fig. 5), CFSE labeled DND41 MVs were captured by anti-CD45 actin filaments in solution and then transferred to a HMM coated surface. Epi-fluorescence microscopy using both FITC and TRITC filter sets then clearly revealed CD45+ MV co-localization with a-CD45-actin filaments (Fig. 5a). This suggests extensive cross-linking of actin filaments with the formation of large aggregates.

To assess the specificity of the binding of CD45 positive MVs anti-CD45-actin filaments, two different analyses were performed. First, no co-localization was observed between anti-CD45-actin filaments and CD45 negative MVs, isolated from MG63 cells (Fig. 5b). As a second negative control, CD45 positive MVs were incubated with tetramethylrhodamine isothiocyanate-phalloidin (RhPh) labeled actin filaments (without antibody) in solution. Neither in this case was any non-specific binding of CD45 positive MVs to actin filaments detected (Fig. 5c).

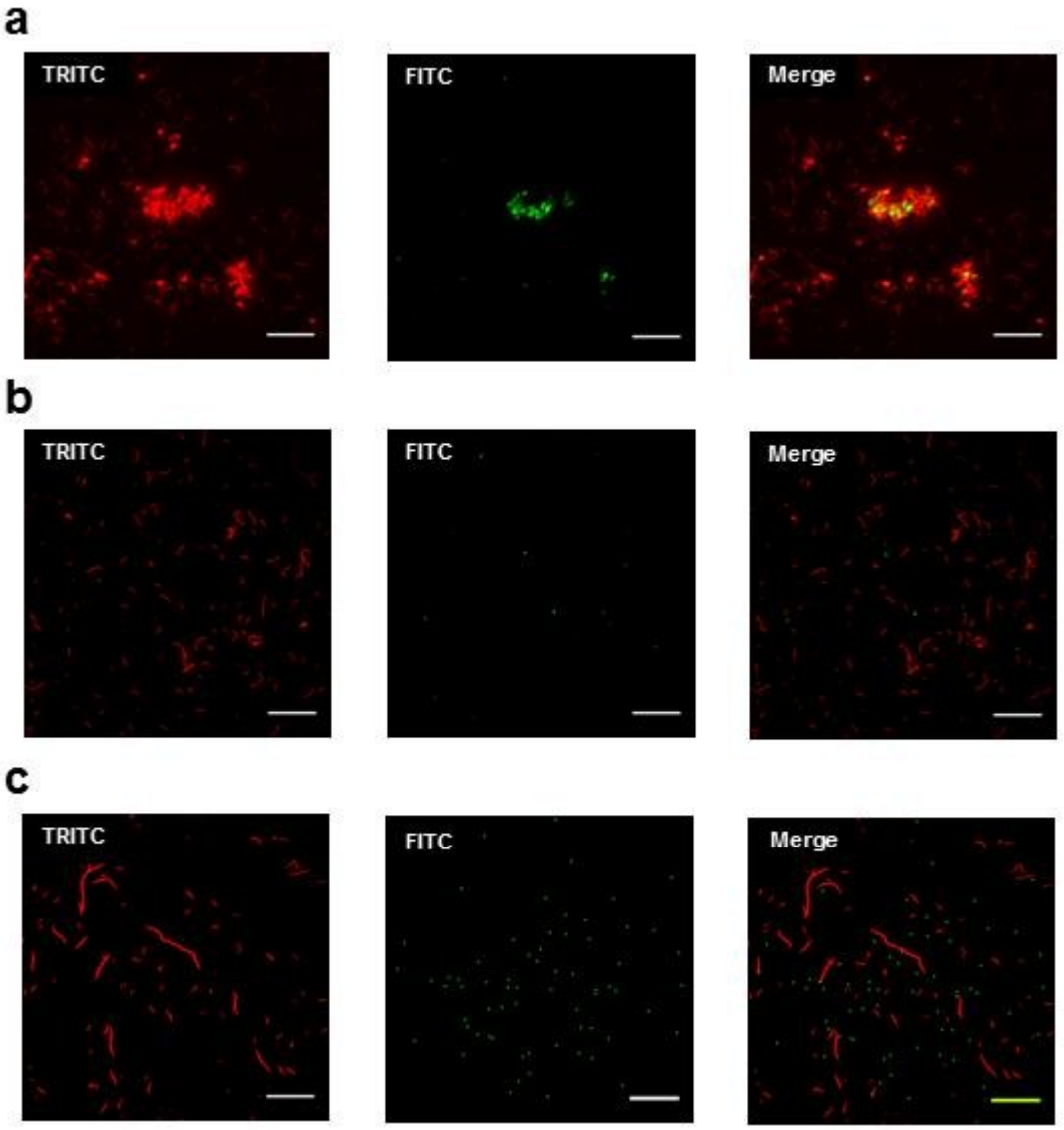

Fig. 5 Co-localization of antibody-conjugated or antibody-free actin filaments (RhPh labeled; TRITC panel, red) and CFSE labeled MVs (FITC panel, green). (a) CFSE labeled CD45+ MVs captured by anti-CD45 conjugated actin filaments. Co-localization (yellow) observed in merged panel. (b) MG63 MVs labeled with CFSE mixed with RhPh labeled and CD45 conjugated actin filaments. Note, no co-localization observed in merged panel. (c) RhPh labeled actin filaments without antibodies mixed with CFSE-labeled and CD45+ MVs. Note, no co-localization observed. Scale bar: 10 µm. Images in (c) subjected to smoothing and brightness adjustment by histogram stretching to reveal weak MV-CFSE fluorescence. The labelling, "FITC" and "TRITC" refer to fluorescence filter used.

Capture and transportation of MVs by anti-CD45-fascin-actin bundles

Anti-CD45 monoclonal antibodies were next incorporated into fascin-actin bundles as described above for a-rIgG. We tested whether these antibodies could capture CD45+ MVs and whether the MVs could be transported by HMM. For this purpose, the HMM coated flow cells were first incubated with fascin-anti-CD45-RhPh actin filament nanocarriers and then with MVs labeled with CFSE. After MgATP addition, the sliding of the nanocarrier was observed (Fig. 6; Movies S5-S6†) using TRITC filter (RhPh labeled) while the possible transportation of MVs bound to carrier was visualized using FITC filter (CFSE labeling). First, in 3 independent experiments (30-39 bundles in each) we found that 27 ± 5.4% (mean ± SEM) of all bundles were associated with at least one CFSE labeled MV. The fraction of motile nanocarriers with or without captured MVs was in these experiments, 0.23 ± 0.09 (mean ± SEM) when a MV was bound to the bundle and 0.28 ± 0.02 otherwise. The velocity (µm s^{-1}

[1]) of anti-CD45 antibody labeled nanocarriers with and without captured MVs was 3.13±0.28 and 3.28±0.11. Thus, both velocity and the fraction of motile carriers were similar in these experiments whether microvesicles were observed to bind to the bundles or not.

However, the fraction of motile nanocarriers was reduced following incubation with MVs (compared to >60% motile fraction without MVs). This suggests that motility inhibition is partly due to the exposure to the MV-containing solution and not due to MV binding per se. However, cross-linking of bundles via microvesicles, with formation of aggregates, also contributes to motility inhibition, at least after some time of sliding (Fig. 6b).

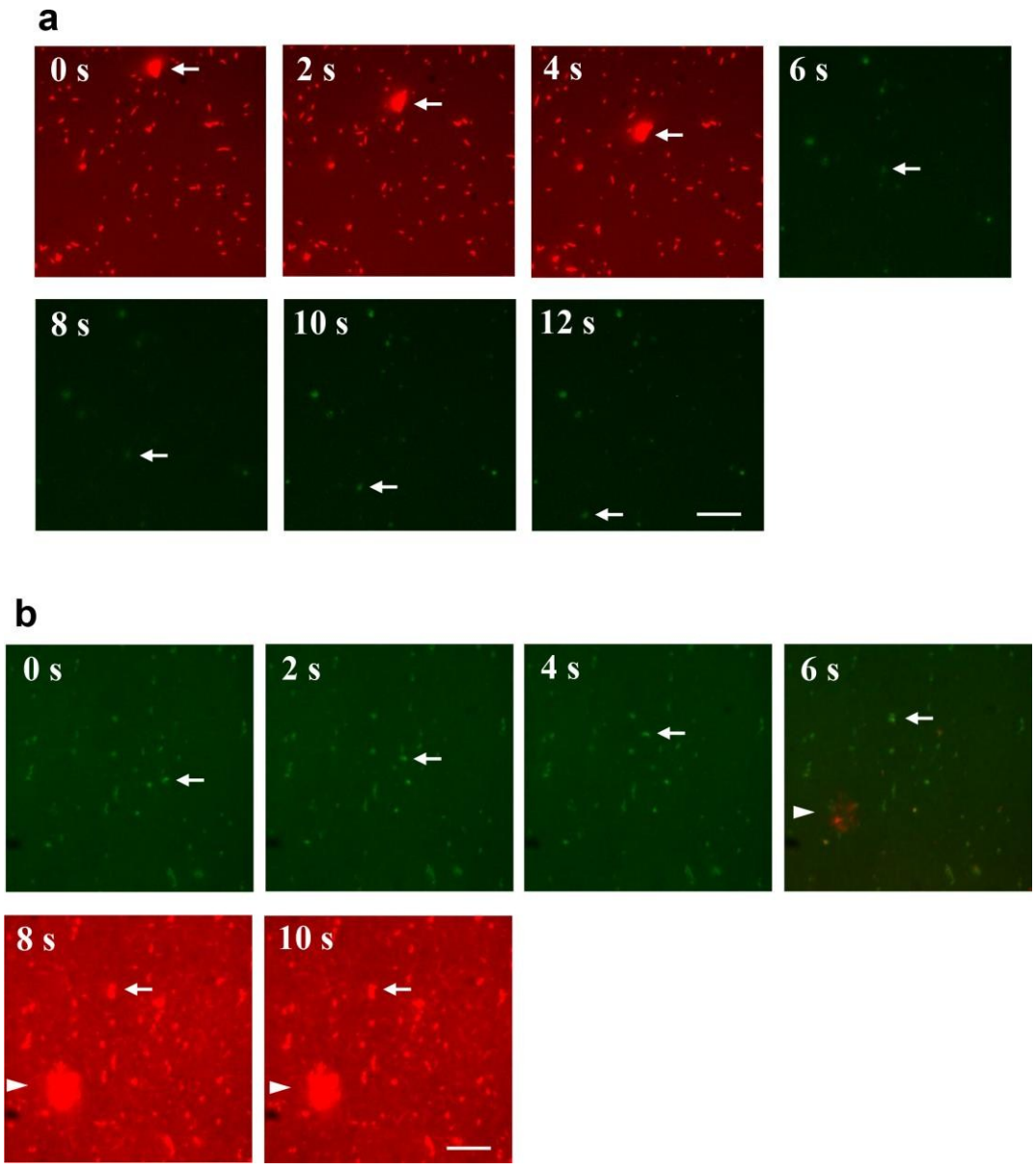

Fig. 6 Image sequences showing HMM propelled microvesicles and aggregation of fascin-actin bundles conjugated by CD45 antibody in the *in vitro* motility assay. (a) Unidirectional movement of bundle (red) carrying microvesicle (green). (b) Small and large aggregates of stationary bundles (red) formed by microvesicles (green) during transport. Bundles (red) and microvesicles (green) were visualized under TRITC and FITC filters, respectively. Switch between filters between 4 and 6 s and 6 and 8 s in A and B, respectively. Arrows and arrowheads denote individual bundles with MVs and stationary bundle-MV aggregates, respectively. Scale bar: 10 µm.

Key findings and relation to previous results

A central finding is the effective incorporation of antibody-conjugated actin filaments into fascin-actin bundles to form a novel complex biopolymer nanocarrier. This carrier exhibited maintained fast actomyosin driven transportation and an unprecedented maximum capacity to transport protein antigens.[14, 22] A second key finding is the observation, for the first time, of the MV capture by monoclonal antibodies on filaments and bundles and aggregation of these filaments/bundles via the MVs. Particularly, the aggregation in solution is the first experimental verification of a recently patented idea for biosensing[23] and our results demonstrate the potential of this approach in detection of the emerging class of vesicular biomarkers.[33]

The HMM driven velocity of bundles that carried protein antigen was reduced by increased incubation concentration but the effects on motility were minimal after 1 min incubationat concentrations of 1 nM or less. The statistically significant effects on velocity and fraction of motile filaments seen in the 1-10 nM range could be useful as a basis for biosensing applications.[47] On the other hand, the minimal effects on motility at sub-nM concentration are also important by enabling use of the nanocarrier in rapid nanoseparation and concentrator nanodevices.[8, 18] At higher Rh-rIgG binding the fraction of motile nanocarriers was reduced as well as the sliding velocity but transport was occasionally maintained for an analyte/G-actin stochiometric ratio up to almost 20%. This is similar to what has been observed for single actin filaments.[14] However, importantly, with the bundles it corresponds to as much as one analyte molecule every 1 nm (about 250 fluorophores per diffraction limited spot of 250 nm with bundle diameter < 100 nm). This can be compared to only 1 per about 20 nm for single actin filaments and microtubules.[22] That is, the bundles provide 20-fold increased maximal binding and transportation capacity per unit length. This explains that all bundles had bound fluorescent analyte after 1 min incubation with protein antigen at 10 nM concentration and that the limit of detection was improved one order of magnitude compared to single filaments (see also[14]).

Our results suggest that the average antigen binding capacity of the antibodies on nanocarries is at least as good as for antibodies on isolated single filaments despite expected complications due to inaccessibility to the bundle interior (see above). This may be due to more effective two-dimensional diffusional search on the bundle surface compared to a filament surface,[48] or to preferential location of antibodies on the outside surface of the bundles.

Binding and transport of MVs has not been attempted previously whether microtubules, actin filaments or actin bundles have been used as shuttles. On the other hand, lipid vesicles of simple composition and with attachment to biotinylated single actin filaments via streptavidin, appreciably compromised motility of isolated filaments[27, 49] but not of fascin-actin bundles.[27] The latter finding is in contrast to the rather poor transportation of MVs observed here, probably reflecting the complexity of our cell-derived system compared to lipid vesicles.

Mechanism of motility inhibition with increased analyte concentration

Fascin cross-links actin filaments in a parallel arrangement, with the same polarity of all filaments, i.e. with all rapidly polymerizing plus ends of individual filaments in the same direction.[28, 31, 46] This arrangement is the basis for the effective transportation[28, 31] of fascin-actin bundles by myosin motor fragments in the in vitro motility assay. Due to the large size of antibodies compared to fascin one would expect a disturbance in the ordered arrangement. Because the largest HMM-transported bundles contained 24 filaments, several filaments must, in this case, be in the bundle interior. With an inter-filament distance of ~8 nm[50] determined by the size of the fascin cross-links there would be little room for antibodies (dimensions 14 x 8 x 4 nm^3).[51] This either implies disturbances of the parallel arrangement of the actin filaments which in that case may have detrimental effects on motile function. Alternatively, antibodies attached to actin filaments are mainly on the bundle surface (see above). The fact that bundle integrity was well maintained with antibody conjugation is consistent with the second alternative. This alternative is also consistent with well-maintained motility[49] in the absence of antigen capture and for occasional large motile filaments. This idea also fits with considerations that the energetic penalty of bundle formation would be lowest with the covalently attached antibodies pointing outwards. We therefore conclude that antibody induced disturbances in internal bundle structure has negligible effect on motility quality.

Instead we considered the possibility that a large fraction of the antibodies and bound antigen on the outside of the bundles inhibits actin-HMM interactions. Fluorescence data cannot distinguish between fluorophores in the interior of bundles and on their surface. This suggests that the stoichiometric ratio between analyte molecules (preferably on the bundle surface) and actin subunits (distributed uniformly over the bundle cross-section) is higher on the bundle surface than overall (i.e. > 0.15). Therefore, the antibodies and their bound protein antigens most likely block an appreciable fraction of the actin monomers from HMM binding. Whereas this may be a factor behind motility inhibition at high Rh-rIgG loading of the bundles, we found no mandatory motility inhibition under these conditions of maximum labeling. This accords with recent findings[49] where streptavidin was linked to 1/5 of the actin monomers on biotinylated actin filaments without reduction in sliding velocity.

One may then ask why the fraction of motile nanocarriers and their velocity was reduced with increased analyte concentration. After discarding the above suggestions we attribute this finding to two mechanisms. First, several bundles and filaments become cross-linked to each other via Rh-rIgG molecules due to polyclonal a-rIgG antibodies on the bundles/filaments (Fig. 5). Unlike the isolated fascin-actin bundles, these higher order structures do not have all actin

filaments oriented in parallel and with their fast-growing plus end in one direction. Clearly, since the actin polarity determines the sliding direction with myosin II walking towards the plus end of actin filaments, such non-polar aggregates will inhibit motility. Second, motility may also be inhibited if antibodies on filaments and bundles cross-link to analytes non-specifically bound to HMM or to the underlying motility assay surface. Antibodies on the surface of the fascin-actin bundles that are oriented downwards towards the HMM layer will not be readily reached by diffusion during the incubation period. Upon addition of ATP and gliding to other areas they may therefore bind surface adsorbed analyte molecules, causing inhibition of motility in analogy to what is seen with so called loaded motility assays.[52] That the density of surface adsorbed analyte molecules is increased at high analyte incubation concentration was apparent from fluorescence micrographs (Fig. S4†).

Cross-linking of different bundles via antigen was observed to even higher degree in attempts to transport microvesicles. However, also other factors may contribute to poor motility in this case such as the lipid composition of the microvesicles. The fact that the negatively charged actin filaments with anti-CD45 antibodies formed cross-links with CD45-positive but not with CD45-negative microvesicles is consistent with evidence[53] that the microvesicles predominantly express negatively charged phospholipids on their surface. This finding is of importance for detection schemes that rely on cytoskeletal filament aggregation[23] via antibodies on the filaments/bundles and antigen on MV surfaces. If the MVs instead had exhibited positive surface charge, non-specific aggregation via negatively charged actin filaments would be expected.[54] On the other hand, for detection schemes relying on transportation,[6, 8, 17, 18] the negative surface charge may be detrimental by binding of MVs to the positively charged actin binding region of myosin.[54] The fact that transportation of MVs could be observed occasionally may be explained by MV attachment to the bundle in a way that prevents contact with the myosin coated surface or that the particular MV has different surface properties than the majority of the MV. A related factor that needs to be considered is the isoelectric point (pI) of the IgG antibodies that may vary between 5 and 9.[55] We did not measure pI but lack of effect of antibody conjugation on myosin driven motility and actin-myosin binding, which depend strongly on electrostatic interactions[56], suggest that antibody conjugation does not substantially modify the electrostatic properties of actin filaments/bundles. A final factor that may be operational in explaining motility inhibition after addition of MVs is rupture of MVs to release proteins from their interior. This is consistent with the inhibition of motility also of those bundles that were not observed to have bound MVs and with recent findings of motility inhibition upon addition of cytosolic protein components to motility assays.

With regard to detection by filament aggregation, it is important to exclude presence of aggregates or aggregate-like structures e.g. by incomplete resuspension of MV pellets during the enrichment phase. However, this risk was considered and minimized and we did not observe any aggregates immediately after resuspension. One may also consider the risk of fusion of several small vesicles, mimicking aggregate formation, as previously shown for phosphatidylserine containing liposomes[57]. However, we did not include Ca^{2+} in the buffer which was important in mediating fusion in the previous studies. Furthermore, importantly, we did not observe aggregate-like assemblies of MVs in the absence of actin filaments/bundles with specific anti-CD45 antibodies (Fig. 5). Nevertheless, in a future device it will be important to rule out any form of non-specific aggregation or membrane fusion effects. Therefore, proper negative controls (as in Fig. 5) need to be integrated with the system at all times. Furthermore, conditions will be optimized to prevent aggregation and membrane fusion (e.g. low Mg^{2+} and Ca^{2+} concentrations).

Towards practical diagnostics applications

A range of detection principles that take advantage of specific properties of cytoskeletal filaments and of motor driven nanoseparation and concentration to detector areas have been suggested for use in diagnostics applications.[6, 8, 10, 12, 18, 23, 26, 58-60] Out of these principles, filament or bundle aggregation via analytes,[23] such as observed here with MVs, has however, not been observed to any useful degree previously. The large aggregates formed between filaments and MVs in solution or between bundles and MVs on the motility assay surface, signal the presence of analyte (MVs) without the need to fluorescence-label these. Effective detection of the aggregates in solution will be feasible by pelleting using a simple table-top centrifuge followed by observation of fluorescence attributed to the large number of fluorophores on the actin filaments. This procedure is facilitated by novel methods[53] for isolation and effective pre-concentration of microvesicles.

In contrast to the MV data, our results with protein antigen show that the use of fascin-actin-antibody nanocarriers will enhance motor driven nanoseparation/concentration procedures due to appreciably improved antigen binding capacity compared to single filaments and maintained high actomyosin velocity at low antigen labeling. The data in Fig. 2 show about ten-fold improvement in sensitivity by switching from filaments to bundles. Further, optimizations to achieve picomolar to femtomolar sensitivity for protein antigens will require a range of routine tests. However, it is obvious that a ten-fold increase of the incubation time would increase sensitivity about ten-fold by increased antigen binding to the bundles. A further ten-, to hundred-fold improvement in detection limit would be achieved using motor-driven nanoseparation and concentration methods.[8, 18] This may be further improved using enhanced fluorescence detection approaches[20, 60-62] and elimination of background fluorescence as well as magnetic pre-separation steps.[63]

Conclusions

We have demonstrated production of high-capacity nanocarriers in the form of fascin-actin bundles covalently conjugated with antibodies. The nanocarrier shows unprecedented maximum antigen carrying capacity for protein antigens and combines advantages of actin-, and microtubule based systems, e.g. the speed is similar to that of myosin propelled actin filaments whereas the flexural rigidity is similar to that of microtubules. In addition to the expected usefulness in nanoseparation and concentration devices for high-sensitivity detection of protein antigens we have also demonstrated the usefulness for specific detection of antigen presenting MVs by aggregation via these vesicles. In this scheme, the fluorescence labeled filaments/bundles contain thousands of APh dye molecules thereby also serving as bright reporter elements, substituting potentially toxic inorganic nanoparticles.

Experimental section

Protein preparations and in vitro motility assays

Actin filaments and heavy meromyosin (HMM) proteolytically derived from myosin II from fast rabbit skeletal muscle were prepared as described previously.[14, 64,65] All experiments using animal material were performed in accordance with national and EU-legislation and were approved by the Regional Ethical Committee for Animal experiments (reference # 96-11), Linköping, Sweden. The actin filaments were labeled by using APh or RhPh (both from Molecular Probes Invitrogen, Eugene, OR). In vitro motility assays with actin filaments propelled by HMM (room temperature: 21–23 ^{o}C) were performed as described recently. Briefly, flow cells, with trimethylchlorosilane (TMCS) derivatized coverslips as HMM binding substrate,[14] were incubated with HMM (120 µg/ml), followed by blocking with bovine serum albumin (BSA) before adding fluorescent actin filaments and ATP-containing assay solution.[14, 64] The latter contained 1 mM MgATP and had an ionic strength of 60 mM. After the standard incubation for an in vitro motility assay, we added antigen, either with Rh-rIgG for 1 min or with DND41 MVs or MG63 MVs for 5 min.

Antibodies conjugated to F-actin and formation of fascin:actin bundles

F-actin was conjugated with a-rIgG (Rockland Immunochemicals, Gilbertsville, USA) or a-CD45 monoclonal antibody (Universal Biologicals LTD, Cambridge, UK) using heterobifunctional cross-linkers[14] followed by assembly into fascin-actin bundles. In brief, non-conjugated or antibody-conjugated F-actin (0.25 mg mL^{-1}; 6 µM on monomer basis) with fluorescent phalloidin (RhPh or APh) in labeling buffer (10 mM 3-morpholinopropane-1-sulfonic acid (MOPS), 60 mM KCl, 2 mM $MgCl_2$, 0.1 mM K_2-ethylene glycol tetraacetic acid (EGTA), 3 mM NaN_3) was gently mixed with His-tagged fascin (Novus Biologicals, Novus Europe, UK) in 20 mM Tris-HCl buffer (including 100 mM NaCl, 2 mM dithiothreitol (DTT) and 20% glycerol), followed by overnight incubation at 4 °C. The procedure is schematically illustrated in Fig. 1. The solutions contained actin and fascin in molar ratios of 1:1 and 1:2 for F-actin-a-rIgG and F-actin-a-CD45, respectively. This is expected[28] to produce fascin-actin bundles containing act and fascin at 4:1 and 2:1 molar ratios. The bundles were store on ice before use in experiments and protein concentrations were measured by Bradford assay.

Analysis of antibody incorporation and protein antigen-binding t filaments and bundles

The degree of incorporation of actin filaments conjugated wi n a-rIgG into fascin-actin bundles was evaluated by detection o Rh-rIgG binding. Here, the fluorescence intensity due to Rh-rIgG reflects the number of a-rIgG molecules with antig binding capacity. For these analyses, the flow cells were pr incubated as for a standard in vitro motility assay befo a addition of, fascin-a-rIgG-actin bundles (60 nM; labeled with APh). Image sequences were recorded using an EMC D camera as described above and fluorescence intensity per rhodamine molecule was estimated from the fluoresc ce intensity per actin filament length assuming 362 fluoresc phalloidins per 1 µm of the actin filament. The number o fluorescent antigens per bundle and the antibody/actin subunit ratio were then calculated from the corrected (Fig. S9†) ratio of the background subtracted Rh-rIgG and A fluorescence intensities. In this process bleed-through effect due to APh fluoresence in the TRITC filter-set, were too sm ll to be of significance when analyzing week Rh-fluorescence.

Cell culture and screening of cell lines for CD45 expression

Human leukemic cell lines were purchased from DSMZ German Collection of Microorganisms and Cell Cultures (Braunschwe g, Germany) while the MG63 osteosarcoma cell line was purchased from ATCC (Manassas, VA, USA). B leukemic c ll lines SEM and RS(4;11) and T leukemic cell lines P12 ICHIKAWA, TALL1, CEM, MOLT3 and DND41 were cultured n RPMI 1640 (GIBCO, Invitrogen Life Technologies, Carlsbad, CA, USA) with 10% fetal calf serum (FCS), L-glutamine (2 mM; GIBCO), penicillin (100U/ml; GIBCO) and streptomycin (00 µg/ml; GIBCO), and maintained at 37 °C in a humidified atmosphere with 5% CO_2. MG63 cells were maintained in DMEM 1X (GIBCO) supplemented with 10% FCS, L-glutamin mM; GIBCO), penicillin (100U/ml; GIBCO) and streptomyci (100 µg/ml; GIBCO), at 37 °C in a humidified atmosphere wi h 5% CO_2. In order to detect cells with CD45 expression, w stained cell pellets with anti-human CD45 monoclonal antibody (Beckman Coulter, Inc., Miami, FL) and CD45 expression was detected by flow cytometry (Fig. S5-S6†).

MVs isolation from cell lines

For MVs isolation, culture medium was centrifuged twice at 2500 g for 15 minutes to remove cells and bigger bodies. Cell-free media was filtered by means of a 1.2 µm size cut-off fil followed by centrifugation at 18000 g for 1 h at 4 Importantly the latter step leaves all vesicles smaller than 0.1

µm (such as exosomes) in the supernatant. This means (considering the previous filtering step) that MVs with a diameter between 0.1 and 1.2 µm were recovered as pellet. The latter was carefully re-suspended in PBS (1X, pH 7.4; GIBCO).

MVs staining and detection by flow cytometry and fluorescence microscopy

To detect MVs by flow cytometry (FACS ARIA III, Becton Dickinson), MVs were stained using the cytoplasmic dye CFSE (1 µM; CellTrace™ CFSE Cell Proliferation Kit, Molecular Probes, Invitrogen, Eugene, OR). The CFSE is retained in MVs for long time due to covalent coupling with intravesicular molecules. In order to check for the presence of CD45, MVs were also stained with anti-human CD45 monoclonal antibody (Beckman Coulter, Inc.) following the manufacturer's instructions and then detected by FACS (Fig. S7-S8†).

For motility assays, CFSE+ MVs were suspended in MOPS buffer (buffer A; cf. Fig. S10†). For fluorescence microscopy based detection of MVs on the HMM coated surface, CFSE staining was optimized, increasing the CFSE incubation concentration to 10 µM to better discriminate MVs from background (Fig. S11†). Another centrifugation step and CFSE+ MVs resuspension in PBS 1X was also added after the staining. Once isolated, CFSE+MVs were stored in PBS 1X at 4 °C for up to 2 weeks before use (Fig. S12†).

The number of MVs present in a microscope image (84 x 84 μm^2) was obtained using an inverted fluorescence microscope (Eclipse TE300, Nikon, Tokyo, Japan) equipped with a Nikon 100x objective (NA 1.4 and a CCD camera (C9100-12, Hamamatsu, Hamamatsu City, Japan).

Analysis of MV-binding to filaments and bundles in solution

For studies of MV binding to actin filaments and fascin-actin bundles, the following mixtures were prepared: (i) DND 41-MVs (10 µl) mixed with a-CD45 actin filaments (6.25 µl) (ii) MG63-MVs (10 µl) mixed with a-CD45-actin filaments (6.25 µl) and (iii) DND 41-MVs (10 µl) mixed with actin filaments without antibodies (6.25 µl). Subsequently 108 µl of buffer D (buffer A with 1 mM DTT) was added followed by incubation for 15 min at 21-23 ^{o}C. Flow cells (see above), for observation of the mixtures, were pre-incubated as for a standard in vitro motility assay until the step before addition of fluorescent actin filaments. At this point we instead incubated with one of the mixtures i-iii for 3 min, followed by wash with buffer D, and addition of r60 solution (buffer A with 10 mM DTT, 35 mM KCl, ionic strength 60 mM) supplied with an anti-bleach system (final activity concentrations of 3 mg mL^{-1} glucose, 20 U mL^{-1} glucose oxidase and 870 U mL^{-1} catalase). The co-localization between actin filaments and MVs was observed using epi-fluorescence microscopy with TRITC and FITC filter sets (details in ESI†; exemplified in Fig. 5 below).

Data analysis

Velocities of single F-actin or fascin-actin bundles were measured using a tracking program developed in a Matlab environment (The MathWorks Inc, Natick, MA).[66] Linear and non-linear curve fittings were performed using Graphpad Prism software (version 6.0, Graphpad software, CA). Image J and Fiji software (Rasband, W.S., ImageJ, U. S. National Institutes of Health, Bethesda, Maryland, USA, http://imagej.nih.gov/ij/, 1997-2012.) were used for analyses of brightness as well as for thresholding and superimposition of images.

Conflict of interest

Alf Månsson is a co-founder, co-owner and CEO of the start-up company ActoSense Biotech AB (Kalmar, Sweden) aiming to develop diagnostic devices based on the aggregation of cytoskeletal elements, particularly actin filaments, in solution. Moreover, A Månsson holds two Swedish patents as well as one US and one European patent in this field.

Acknowledgements

This work was funded by The European commission (FP7) under the contract MONAD (NMP4-SL-2009-228971), The Carl Trygger Foundation, The Swedish Research Council (Project 621-2010-5146), The Faculty of Natural Sciences and Engineering and the Faculty of Health and Life Sciences at Linnaeus University.

S.K. thanks SERB-DST, Govt. of India for the award of Fast Track Young Scientist. We thank Prof. Kazuhiro Kohama, Gunma University, Japan for suggestions and discussions about fascin-actin bundle experiments. Finally, we would like to thank Camilla Mohlin at Linnaeus University, Kalmar for help with cell culturing.

Notes and references

1. D. A. Giljohann and C. A. Mirkin, *Nature*, 2009, **462**, 461-464.
2. G. M. Whitesides, *Nature*, 2006, **442**, 368-373.
3. J. V. Jokerst, J. W. Jacobson, B. D. Bhagwandin, P. T. Floriano, N. Christodoulides and J. T. McDevitt, *Anal Chem*, 2010, **82**, 1571-1579.
4. P. E. Sheehan and L. J. Whitman, *Nano Lett*, 2005, **5**, 803-807.
5. S. T. Yang, Y. Liu, Y. W. Wang and A. Cao, *Small*, 2013, **9**, 1635-1653.
6. T. Fischer, A. Agarwal and H. Hess, *Nat Nanotechnol*, 2009, **4**, 162-166.
7. P. Katira and H. Hess, *Nano Lett*, 2010, **10**, 567-572.
8. C. T. Lin, M. T. Kao, K. Kurabayashi and E. Meyhofer, *Nano Lett*, 2008, **8**, 1041-1046.
9. Y. M. Huang, M. Uppalapati, W. O. Hancock and T. J. Jackson, *Biomed Microdevices*, 2007, **9**, 175-184.
10. T. Korten, A. Månsson and S. Diez, *Current Opinion in Biotechnology* 2010, **21**, 477-488.
11. D. Steuerwald, S. M. Fruh, R. Griss, R. D. Lovchik and V. Vogel, *Lab on a chip*, 2014, **14**, 3729-3738.

12. S. Ramachandran, K. H. Ernst, G. D. Bachand, V. Vogel and H. Hess, *Small*, 2006, **2**, 330-334.
13. C. M. Soto, B. D. Martin, K. E. Sapsford, A. S. Blum and B. R. Ratna, *Anal Chem*, 2008, **80**, 5433-5440.
14. S. Kumar, L. ten Siethoff, M. Persson, M. Lard, G. te Kronnie, H. Linke and A. Månsson, *PLOS One*, 2012, **7**, e46298.
15. S. Diez, C. Reuther, C. Dinu, R. Seidel, M. Mertig, W. Pompe and J. Howard, *Nano Letters*, 2003, **3**, 1251-1254.
16. S. Hiyama, R. Gojo, T. Shima, S. Takeuchi and K. Sutoh, *Nano Letters*, 2009, **9**, 2407-2413.
17. P. Katira and H. Hess, *Nano Lett*, 2010, **10**, 567-572.
18. M. Lard, L. Ten Siethoff, S. Kumar, M. Persson, G. Te Kronnie, H. Linke and A. Mansson, *Biosens Bioelectron*, 2013, **48**, 145-152.
19. H. Hess, J. Clemmens, D. Qin, J. Howard and V. Vogel, *Nano Letters*, 2001, **1**, 235-239.
20. A. Månsson, M. Sundberg, M. Balaz, R. Bunk, I. A. Nicholls, P. Omling, S. Tågerud and L. Montelius, *Biochem Biophys Res Commun*, 2004, **314**, 529-534.
21. S. Korten, N. Albet-Torres, F. Paderi, L. Ten Siethoff, S. Diez, T. Korten, G. Te Kronnie and A. Mansson, *Lab on a chip*, 2012, **DOI:10.1039/C2LC41099K**.
22. C. M. Soto, B. D. Martin, K. E. Sapsford, A. S. Blum and B. R. Ratna, *Anal Chem*, 2008, **80**, 5433-5440.
23. A. Månsson and S. Tågerud, *US patent*, 2014, **US 8,658,381**
24. A. Agarwal and H. Hess, *Prog Polymer Sci*, 2010, **35**, 252-277.
25. T. Nitta, A. Tanahashi, Y. Obara, M. Hirano, M. Razumova, M. Regnier and H. Hess, *Nano Lett*, 2008, **8**, 2305-2309.
26. T. Nitta and H. Hess, *Cell Mol Bioeng*, 2012, **6**, 109-115.
27. H. Takatsuki, H. Tanaka, K. M. Rice, M. B. Kolli, S. K. Nalabotu, K. Kohama, P. Famouri and E. R. Blough, *Nanotechnology*, 2011, **22**, 245101
28. H. Takatsuki, E. Bengtsson and A. Mansson, *Biochim Biophys Acta*, 2014, **1840**, 1933-1942.
29. H. Takatsuki, K. M. Rice, S. Asano, B. S. Day, M. Hino, K. Oiwa, R. Ishikawa, Y. Hiratsuka, T. Q. Uyeda, K. Kohama and E. R. Blough, *Small*, 2010, **6**, 452-457.
30. M. M. Claessens, M. Bathe, E. Frey and A. R. Bausch, *Nat Mater*, 2006, **5**, 748-753.
31. R. Ishikawa, T. Sakamoto, T. Ando, S. Higashi-Fujime and K. Kohama, *J Neurochem*, 2003, **87**, 676-685.
32. E. M. DelaCruz and T. D. Pollard, *Biochemistry*, 1996, **35**, 14054-14061.
33. G. Raposo and W. Stoorvogel, *J Cell Biol*, 2013, **200**, 373-383.
34. G. Turturici, R. Tinnirello, G. Sconzo and F. Geraci, *Am J Physiol. Cell physiol*, 2014, **306**, C621-633.
35. Y. J. Yoon, O. Y. Kim and Y. S. Gho, *BMB reports*, 2014, **47**, 531-539.
36. Y. Lee, S. El Andaloussi and M. J. Wood, *Hum mol gen*, 2012, **21**, R125-134.
37. C. Tetta, E. Ghigo, L. Silengo, M. C. Deregibus and G. Camussi, *Endocrine*, 2013, **44**, 11-19.
38. J. Ratajczak, K. Miekus, M. Kucia, J. Zhang, R. Reca, P. Dvorak and M. Z. Ratajczak, *Leukemia*, 2006, **20**, 847-856.
39. A. L. Revenfeld, R. Baek, M. H. Nielsen, A. Stensballe, K. Varming and M. Jorgensen, *Clinical therapeutics*, 20[illegible], **36**, 830-846.
40. Y. Sun and J. Liu, *Clinical therapeutics*, 2014, **36**, 863-87[illegible]
41. V. R. Martins, M. S. Dias and P. Hainaut, *Curr Opin Oncol*, 2013, **25**, 66-75.
42. V. R. Minciacchi, M. R. Freeman and D. Di Vizio, *Seminars in cell & developmental biology*, 2015, **40**, 41-51.
43. A. Grotzky, Y. Manaka, T. Kojima and P. Walde, *Biomacromolecules*, 2011, **12**, 134-144.
44. G. Iyer, F. Pinaud, J. Xu, Y. Ebenstein, J. Li, J. Chang, [illegible] Dahan and S. Weiss, *Bioconjug Chem*, 2011, **22**, 100[illegible] 1011.
45. J. Y. Byeon, F. T. Limpoco and R. C. Bailey, *Langmuir*, 2010, **26**, 15430-15435.
46. M. M. Claessens, C. Semmrich, L. Ramos and A. R. Bausch, *Proc Natl Acad Sci U S A*, 2008, **105**, 8819-8822.
47. T. Korten and S. Diez, *Lab on a chip*, 2008, **8**, 1441-1447.
48. H. C. Berg and E. M. Purcell, *Biophys J*, 1977, **20**, 193-[illegible].
49. M. Persson, M. Gullberg, C. Tolf, A. M. Lindberg, A. Mansson and A. Kocer, *PloS one*, 2013, **8**, e55931.
50. S. Jansen, A. Collins, C. S. Yang, G. Rebowski, T. Svitkina and R. Dominguez, *J Biol Chem*, 2011, **286**, 30087-300[illegible]
51. V. R. Sarma, Silverto.Ew, D. R. Davies and W. D. Terry, *J Biol Chem*, 1971, **246**, 3753-&.
52. W. Bing, A. Knott and S. B. Marston, *Biochem J*, 200[illegible], **350**, 693-699.
53. Z. Brownlee, K. D. Lynn, P. E. Thorpe and A. J. Schroit, *J Immunol Methods*, 2014, **407**, 120-126.
54. N. Albet-Torres, A. Gunnarsson, M. Persson, M. Balaz, J. Hook and A. Mansson, *Soft Matter*, 2010, **6**, 3211-3219.
55. S. Takahashi, N. Wada, K. Harada and M. Nagata, *Kidney international*, 2004, **66**, 1556-1560.
56. M. A. Geeves, R. Fedorov and D. J. Manstein, *Cell Mol Life Sci*, 2005, **62**, 1462-1477.
57. S. T. Sun, C. C. Hsang, E. P. Day and J. T. Ho, *Biochim Biophys Acta*, 1979, **557**, 45-52.
58. T. Kim, L. J. Cheng, M. T. Kao, E. F. Hasselbrink, L. Guo a[illegible] E. Meyhofer, *Lab on a chip*, 2009, **9**, 1282-1285.
59. M. G. van den Heuvel, M. P. de Graaff and C. Dekker, *Science*, 2006, **312**, 910-914.
60. L. Ten Siethoff, M. Lard, J. Generosi, H. S. Andersson, H. Linke and A. Mansson, *Nano letters*, 2014, **14**, 737-742.
61. M. Lard, L. Ten Siethoff, A. Månsson and H. Linke, *Sci Rep*, 2013, **3** 1092.
62. D. Axelrod, *Methods Enzymol*, 2003, **361**, 1-33.
63. S. Kumar, L. ten Siethoff, M. Persson, N. Albet-Torres, A. Mansson, *J Nanobiotechnol*, 2013, **11**.
64. S. J. Kron, Y. Y. Toyoshima, T. Q. Uyeda and J. A. Spudich, *Methods Enzymol*, 1991, **196**, 399-416.
65. J. D. Pardee and J. A. Spudich, *Method Cell Biol*, 1982, **24**, 271-289.
66. A. Mansson and S. Tagerud, *Anal Biochem*, 2003, **3[illegible]**, 281-293.

Journal Name

ARTICLE